



Efficient geomorphological mapping based on geographic information systems and remote sensing data: an example from Jena, Germany

Ikram Zangana, Jan-Christoph Otto, Roland Mäusbacher & Lothar Schrott

To cite this article: Ikram Zangana, Jan-Christoph Otto, Roland Mäusbacher & Lothar Schrott (2023): Efficient geomorphological mapping based on geographic information systems and remote sensing data: an example from Jena, Germany, Journal of Maps, DOI: [10.1080/17445647.2023.2172468](https://doi.org/10.1080/17445647.2023.2172468)

To link to this article: <https://doi.org/10.1080/17445647.2023.2172468>



© 2023 The Author(s). Published by Informa UK Limited, trading as Taylor & Francis Group on behalf of Journal of Maps



[View supplementary material](#)



Published online: 06 Mar 2023.



[Submit your article to this journal](#)



Article views: 415



[View related articles](#)



[View Crossmark data](#)



This article has been awarded the Centre for Open Science 'Open Data' badge.



Efficient geomorphological mapping based on geographic information systems and remote sensing data: an example from Jena, Germany

Ikram Zangana ^a, Jan-Christoph Otto ^b, Roland Mäusbacher^c and Lothar Schrott^a

^aDepartment of Geography, University of Bonn, Bonn, Germany; ^bDepartment of Geography and Geology, University of Salzburg, Salzburg, Austria; ^cDepartment of Physical Geography, Friedrich-Shiller University of Jena, Jena, Germany

ABSTRACT

We present a detailed geomorphological map (1:5000-scale) of a middle mountainous area in Jena, Germany. To overcome limitations and to extend the possibility of manually digital mapping in a structural way, we propose an approach using geographic information systems (GIS) and high-resolution digital data. The geomorphological map features were extracted by manually interpreting and analyzing the combination of different data sources using light detection and ranging (LiDAR) data. A combination of topographic and geological maps, digital orthophotos (DOPs), Google Earth images, field investigations, and derivatives from digital terrain models (DTMs) revealed that it is possible to generate the geomorphologic features involved in classical mapping approaches. LiDAR-DTM and land surface parameters (LSPs) can provide better results when incorporating the visual interpretation of multidirectional hillshade and LSP composite maps. Findings enabled us to systematically delineate landforms and geomorphological process domains. We suggest that further use of digital data should be undertaken to support analysis and applications.

ARTICLE HISTORY

Received 1 July 2022
Revised 26 October 2022
Accepted 12 January 2023

KEYWORDS

Geomorphological map;
ArcGIS; remote sensing; Jena;
Germany

1. Introduction

Geomorphological maps are among the best tools for understanding the physical context of features at the Earth's surface. They provide a conventional description of landforms, processes, and near-surface materials (Dramis et al., 2011). In addition to their scientific value, geomorphological maps play a significant role in hazard assessment (Parry, 2011), the visualization of landscape characteristics for education and tourism (Bollati et al., 2017), and land management and planning (Devoto et al., 2012).

Geomorphological maps are traditionally based on manual fieldwork, which can be time-consuming, require significant experience and could provide some pitfalls during the mapping and layout process (e.g. Seijmonsbergen, 2013; Otto et al., 2011). Geomorphological maps can also be purely based on remote-sensing data, like digital elevation models or digital imagery. Field mapping can be less accurate to remotely mapped data, especially in steep and complex terrain, owing to problems of accessibility (Otto & Dikau, 2004; Gustavsson et al., 2008; Beckenbach et al., 2014). Additionally, semi-automatic approaches (e.g. Blaschke, 2010; Drăguț & Eisank, 2012; MacMillan & Shary, 2009; Schnevoigt et al., 2008; Wu et al., 2016; Piloyan & Konečný, 2017; Chen et al., 2018) have been developed to facilitate the generation of

geomorphological information, such as detection and classification of landforms, processes, or geomorphic process units, directly from remote sensing data (e.g. aerial photographs, LiDAR and RADAR [both airborne or satellite-based]). However, accuracy and reliability of semi-automated approaches are often below field and remote mapping approaches and are mostly restricted to selected landforms and processes (Otto & Smith, 2013; Hillier et al., 2015). In addition, Skentos (2018) indicated that despite attempts to generalize the derived algorithms, not all automated procedures are adequate for landform classification under all circumstances.

Remotely sensed data sources have become more extensively available since the middle of the twentieth century (Smith & Pain, 2009). In the late 1990s, high-resolution data including light detection and ranging (LiDAR) has become accessible (Mcdowell, 2013). LiDAR data have improved the description and analysis of Earth's surface processes and landforms (see Hengl & Reuter, 2008; Smith et al., 2011) and provides a sophisticated approach for overcoming some of the issues inherent to classical-based methods, such as time required and quality of data (Beckenbach et al., 2014; Jones et al., 2007). Smith (2011) found that ~2 km² can be mapped per day by an experienced geomorphologist using a traditional field-based

CONTACT Ikram Zangana  ikram.zangana@uni-bonn.de  Ikram Zangana, Meckenheimer Allee 166, 53115 Bonn, Germany

 Supplemental map for this article can be accessed at <https://doi.org/10.1080/17445647.2023.2172468>.

© 2023 The Author(s). Published by Informa UK Limited, trading as Taylor & Francis Group on behalf of Journal of Maps

This is an Open Access article distributed under the terms of the Creative Commons Attribution License (<http://creativecommons.org/licenses/by/4.0/>), which permits unrestricted use, distribution, and reproduction in any medium, provided the original work is properly cited.

method in comparison to $\sim 10\text{--}100\text{ km}^2$ per day for remote digital mapping. According to Schrott et al. (2013), high-resolution remote sensing data, such as LiDAR, has augmented the visualization of terrain. Consequently, geomorphological maps based on remote sensing data, especially high-resolution digital elevation models (DEMs), have increased in the last few decades (Chandler et al., 2018; Garcia & Grohmann, 2019; Gehrman & Harding, 2018; Gustavsson et al., 2006, 2008; Jones et al., 2007; Lambiel et al., 2016; Magliulo & Valente, 2020; Otto et al., 2017; Seijmonsbergen et al., 2011; Seijmonsbergen, 2013). The application of high-resolution data can improve the quality of the product, is less time-consuming, and requires less cost and risk involved in field campaigns (Napieralski et al., 2013).

Visualization techniques provide vital support for manual mapping based on remote sensing and DEM data to enhance the interpretation of landforms and processes (Doneus, 2013; Otto & Smith, 2013; Nagi, 2014; Daxer, 2020). For example, selected land surface parameters (LSPs), including slope (slope gradient, the first derivative of elevation), hillshade, curvature (profile and plan curves, the second derivative of elevation), and composite maps of LSPs, can present valuable visualization techniques to detect the distribution and boundaries of landforms (Anders et al., 2011, 2015). Further research is required to extend the capabilities of visualization techniques and high-resolution data for the generation of geomorphological maps and to improve manual digital mapping approaches in a structured way.

Herein, we present an approach to manual mapping using a combination of high-resolution LiDAR-DTM data, LSPs, topographical maps, geologic maps, digital orthophotos (DOPs), and a set of visualization techniques applied to a low-range mountain area in central Germany. We developed a systematic workflow that can be transferred and implemented to different terrains.

Our study aims to assess the effect of combining various data sources and visualization techniques on the quality and accuracy of the resulting geomorphological map and thereby evaluate the efficacy of such data sources to extract the genesis of geomorphologic processes and landforms.

The map presents geomorphological landscape elements and processes from the Saale valley near Jena and its surrounding slopes and hills at a 1:8000 scale. The high-resolution map provides a key tool for further geomorphological research in the area.

2. Study area

The area is located in the eastern part of Thuringia State, near the city of Jena, in Germany (Figure 1). It is approximately 44 km^2 in size spreading across two different elevation zones. One is a low-elevation area

that includes most of the Saale River valley and parts of the Roda River catchment. The lowest point in this area is about 140 m asl. The other is an elevated zone consisting of a plateau, low mountains, and the adjacent slopes at elevations up to 400 m asl. As part of the Thuringia basin, the study area dominated by two major geological formations. The Muschelkalk formation (limestone) covers the majority of the high-altitude areas, while the Buntsandstein formation (red sandstone) covers the low-altitude areas (Föhlich, 2002; Seidel, 1992).

The city of Jena, in the northwestern part of the study area, demonstrates how human impact on the environment can cause extensive changes in the character of the landscape.

Specifically, most of the flood plain along both the eastern and western sides of the Saale River have been modified by human activities (e.g. buildings, road construction and so on).

The annual mean temperature is between 9°C and 11°C . Summer mean temperature are around 16° and 18° , winter means between 0° and 2° . The mean annual rainfall is between 600 and 800 mm (TMUEN, 2017). Land use is dominated by residentials, industries, and infrastructures in the valley floors and some parts of the gentle slopes. The forests are strongly concentrated on the steepest slopes and top of the plateau. Farmlands are mostly distributed along with the Saale River flood plains and its tributaries. However, to a smaller extent, grasslands/pastures are scattered in the northern half of the study area (TLUBN, 2022). According to the ‘Soil-Geological concept map’ of Thuringia, 1:100,000 (Rau et al., 2000), the soil types in this area include Rendzinas (Leptosols) formed on Muschelkalk formations mainly on the plateau area. Pararendzinas (Pelosols) formed in the Buntsandstein area and on the slopes. However, the Holocene floodplain and flat areas of the region are covered by the Gley-vega soil types (Gleysols). The Braunerde/Braun soils (Cambisols) cover areas where sandstone, sandstone/siltstone, and claystone sequences of the lower and middle Buntsandstein are dominated. Podzols (Podzols) covered some southern parts of the study area.

3. Materials and methods

A LiDAR-DTM with a 2 m cell size was provided by the Thuringian State Office for Soil Management and Geoinformation and used as the base for mapping (TLBG, 2019a). Other data sources used for geomorphological mapping include high-resolution satellite imagery (Google Earth images), DOPs (20 cm cell size) (TLBG, 2019b), a digital topographic map of Thuringia at 1:10,000 scale (DTK10) (TLBG, 2019c), and geologic maps of Thuringia at 1:25,000 and 1:200,000 scales (GK25 & GK200) (TLUBN, 2019).

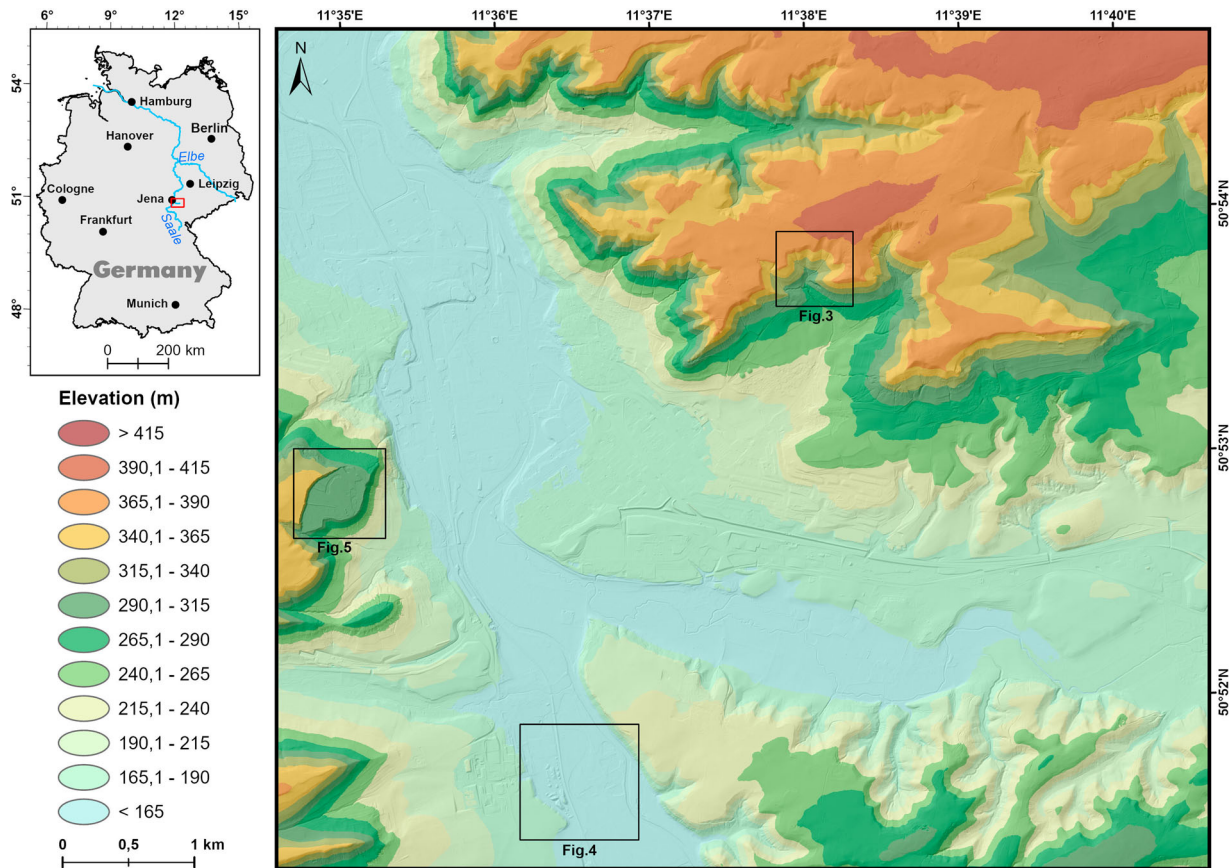


Figure 1. Location of the study area, black squares show the approximate locations of the frames in figures 3, 4 and 5.

Various LSPs were calculated based on DTM using QGIS and ArcGIS (Table 1 and Figure 2). We generated a composite LSP by combining the topographic openness (TO; for more see Daxer, 2020) with slope following the methods of Anders et al. (2011) (refer to Figure 3). In combination with other data sources (e.g. geology, topographic maps and DOPs), DEM derivatives and LSPs were applied to enhance the visualization and detectability of landforms and surface features, especially landforms related to variation across a spatial scale. The TO and LSP composite maps provided a clear distinction between the character of the landform and the surrounding features, also highlighting the highest and lowest parts of landforms (Doneus, 2013), again in comparison to other data sources (Figure 3 and Table 1). In addition, multidirectional hillshade maps are valuable for the visualization of LiDAR-DTMs required for manually analyzing landforms. This raster is created, for example, using ArcGIS Pro by the ‘*Raster Function*’ toolboxes from the ‘*Imagery*’ tool. For visualization, we employed the symbols for geomorphological mapping used by Otto (2008).

Mapping was performed as part of a two-stage procedure (Figure 2). Following the compilation and preparation of the source data, an approach was adopted to generate a geomorphological map in Stage I. Table 1 presents the different data sources and their application in this study. Additionally,

comments on potential limitations of the data to landform detection are listed. Mapping was performed at a high-resolution scale of 1:1000 to obtain greater detail of information (Otto & Smith, 2013).

Stage I comprised two main parts: identifying the genesis of landforms/processes and extracting geomorphologic process domains. Stage I, or the upper part, presents our proposed approach to systematically identify landform genesis. This was conducted *via* evaluation of available data sources and field surveys. For example, if the genesis of a landform were ambiguous, the topographic map needed to be analyzed. In addition, orthophotos was proceeded in some cases. As a last option/solution, a field check could then be required.

In order to identify crests and ridges, we applied focal statistics analyses with varying moving window sizes using the curvature raster as input data (Smith & Clark, 2005; Wood, 1996). Steps and slope breaks were generated manually after visual inspection of the slope layers and classified by calculating the width of the slope breaks based on GIS-DTM data, using ‘*Measure*’ and ‘*3D Analyst*’ toolboxes in ArcMap, for instance, steps class of 2–10 m (for more see Main Map, legend 4). Alluvial fans were mapped from the combination of topographic data and the aid of geologic maps. Since it is impossible to precisely outline an area symbol from the DTM, a point symbol feature was used instead. The hillslope processes &

Table 1. Detailed description of data sources, resolution, the required procedure/application, limitations, and the advantages or improvements for constructing geomorphologic maps.

Data sources	Resolution/ scale	Requirement	Application	Weakness	Strength/improvement
Hillshade and multidirectional hillshade	2 m cell size	QGIS /ArcGIS online (ArcPro), which computes hillshade from six different directions as opposed to the single direction of a default hillshade	To provide <ul style="list-style-type: none"> a quick indication of the terrain on-screen surveys analyzing landforms as a substitute for the field survey a background for other layers to better visualize landforms 	Traditional hillshades are made by illuminating light from the northwest. This frequently results in overexposure of the illuminated sides and obscuration of details in the terrain on non-illuminated sides	<ul style="list-style-type: none"> Promotes the balance between over-exposed and non-illuminated areas, resulting in a more accurate representation of the landscape Can develop on-screen mapping accuracy (Nagi, 2014, Tzvetkov, 2018)
Simple LSPs: 1. Slope	2 m cell size	ArcGIS/QGIS (default algorithm)	<ul style="list-style-type: none"> To provide valuable knowledge to interpret and digitize breaks in slopes on-screen manually To determine the boundaries of landforms 	A single classification interval alone does not provide the necessary information needed for precise interpretation of landforms, because of the morphological difference in landform types and the range of landform sizes (e.g. steps, depressions, and knolls)	Mapping from <ul style="list-style-type: none"> a range of classification intervals instead of a single group (see Jones et al., 2007)
2. Curvature	10 m cell size	ArcGIS and QGIS (default algorithm)	To provide a valuable source for manual landform delineation (e.g. ridges, crests, stream networks, and drainage ways/ adjustments)	A correct landform investigation might be difficult due to the high-resolution of the original DTMs (e.g. 2 m resolution)	To obtain a reasonable raster <ul style="list-style-type: none"> Focal Statistical toolbox processed (e.g. 5 × 5–9 × 9 moving window instead of the default 3 × 3) extract the curvature from a resampled DEM of 10 m
3. Topographic openness (TO)	25 × 25 m, 50 × 50 m, 250 × 250 m	QGIS (for steps see Daxer, 2020)	<ul style="list-style-type: none"> To manually correct landforms that are created based on other parameters To better define landforms boundary 	–	Consider both the highest and lowest parts of landforms (Daxer, 2020 & Meng et al., 2018)
Composite LSPs (slope & TO)	Slope 3 × 3 m with TO25 × 25 m and TO250 × 250 m	Can be obtained by <ul style="list-style-type: none"> QGIS > Plugin > Semiautomatic Classification > RGB ArcGIS > Toolbox > Data Management > Composite Bands <p>Arc Pro > Toolboxes > Data Management > Raster Processing > Composite Bands</p>	When applying it, <ul style="list-style-type: none"> the detection of landforms boundaries is improved in comparison to single LSPs it provides us with greater accuracy and presents the landscape better than those on a single LSP (see Smith et al., 2013) 	–	<ul style="list-style-type: none"> A clear distinction between the landform character and its surrounding features <p>Both the highest and lowest parts of the landform are much better detected (Doneus, 2013) in comparison to other data sources (Figure 5)</p>
Geological map	1:25,000 and 1:200,000	In a digital format such as GK25 or at a better and more detailed scale	It provides valuable information <ul style="list-style-type: none"> by overlaying on other data sources, it can manually define the boundaries of landforms and their geomorphic processes to obtain the genesis of landforms 	When a geological map at a scale of 1:200,000 is required to delineate a detailed map (e.g. at scales of 1:5,000–1:10,000)	When draped over the DEM data and LSPs, manual mapping of landforms and their geomorphological processes boundaries are modified and enhanced

(Continued)

Table 1. Continued.

Data sources	Resolution/ scale	Requirement	Application	Weakness	Strength/improvement
Topographic map	1:10,000	An appropriate scale (e.g. < 1:10,000) and a digital format	Provides preliminary data for <ul style="list-style-type: none"> manually delineating landforms/ processes manually modifying the hydrology layer elements 	If the scale of the topographic map is smaller than that of the targeted map	Scale variation issue improves by modifying the boundaries of landforms and genesis from overlaying it over a DTM and DTM derivatives and by field examination, then considering the objectives of the map
Orthophoto/ Google earth images	0.20 m cell size	A reasonable resolution of about <20 cm	<ul style="list-style-type: none"> Visualize the landscape in 3D and 2D Combine it with other data sources to characterize the feature and its genesis As a substitute for field mapping and to become familiar with the area prior the field checking	When: <ul style="list-style-type: none"> The resolution of the images is coarser than the scale of the map Wherever the image quality is insufficient (e.g. > 20 cm) to examine the landforms of interest	By field examination and by comparison with other data sources

deposits layer including, for example, landslide, debris flow, incision, and alluvial fan (see the Main Map, legend 3), was manually delineated based on the relevant data sources and field check, using a point-based feature.

The hydrological features were digitized using blue color (lines, points, and polygons). Streamlines were extracted from the topographic map and manually corrected based on field observations. Stream types were differentiated between perennial and intermittent based on field surveys. Lakes were extracted by selecting areas bigger than 20 m² where slope values were lesser than 0.5° from the DEM and modified manually using the topographic map. The extraction of sources, waterlogging, and seepages was impossible using LiDAR data only. Hence, we obtained these characteristics from the combination of topographic maps, orthophotos, and field surveys. In contrast, to define and classify pathways, we followed the geomorphological map of Germany (GMK) concept (Barsch & Liedtke, 1985), using different techniques. In the initial step, each valley with a width of <25 m on the ground was identified. In the second step, valley profiles were examined manually using DEM data and the *profile graph* tool (using *3D Analyst* toolbox, ArcMap). Different valley types were classified based on the visual inspection of the cross-profiles designed using our experience.

We employed an approach to determine the predominant landforms and processes in the middle-mountain regions during the early stages of mapping to ensure that irrelevant landforms/processes were not processed (see Figure 2, Stage I/lower part).

In the initial step, a single polygon (color fill) was drawn to cover the entire study area and defined as

a denudational domain by default. This was done by considering the yes/no criteria *via* comparison with other typical characters of occurring geomorphic processes. However, any part of the initial polygon (denudational process domain) was removed, and subsequently substituting it with an active type of a geomorphic process in that domain. For example, the signature of denudation area was replaced with a fluvial process domain wherever fluvial incisions, erosional rims, rivers/streams, and flood plains were identified. Likewise, the topographic map and DOP were analyzed to separate anthropogenic areas (gray polygons) from urban domains (rose-quartz color fill). In other words, anthropogenic activity areas can be divided into two parts: (1) zones that were slightly altered by human activities, which are classified as anthropogenic process domains (see the Main Map, legend 1), and (2) zones that were strongly modified by anthropogenic activities; these were not surveyed and represented by a rose-quartz color-fill polygon. Following a similar procedure, karstic domains were delineated if the area (1) was dominated by the lower Muschelkalk formation (Jena Formation; see the inset geologic map in the Main Map) and (2) was characterized by depressions and undulating topography consistent with gentle slopes. In this way, the loop was continued until the entire study area had been classified. As a result, this layer has been divided into six classes of main geomorphological processes, ten sub-classes of interactive processes domain, and one class for unsurvey areas.

During Stage II (Figure 1), various parts of the study area were checked in the field. Two field checks were carried out with the support of a differential GPS (DGPS). Field surveys were prepared by accessing

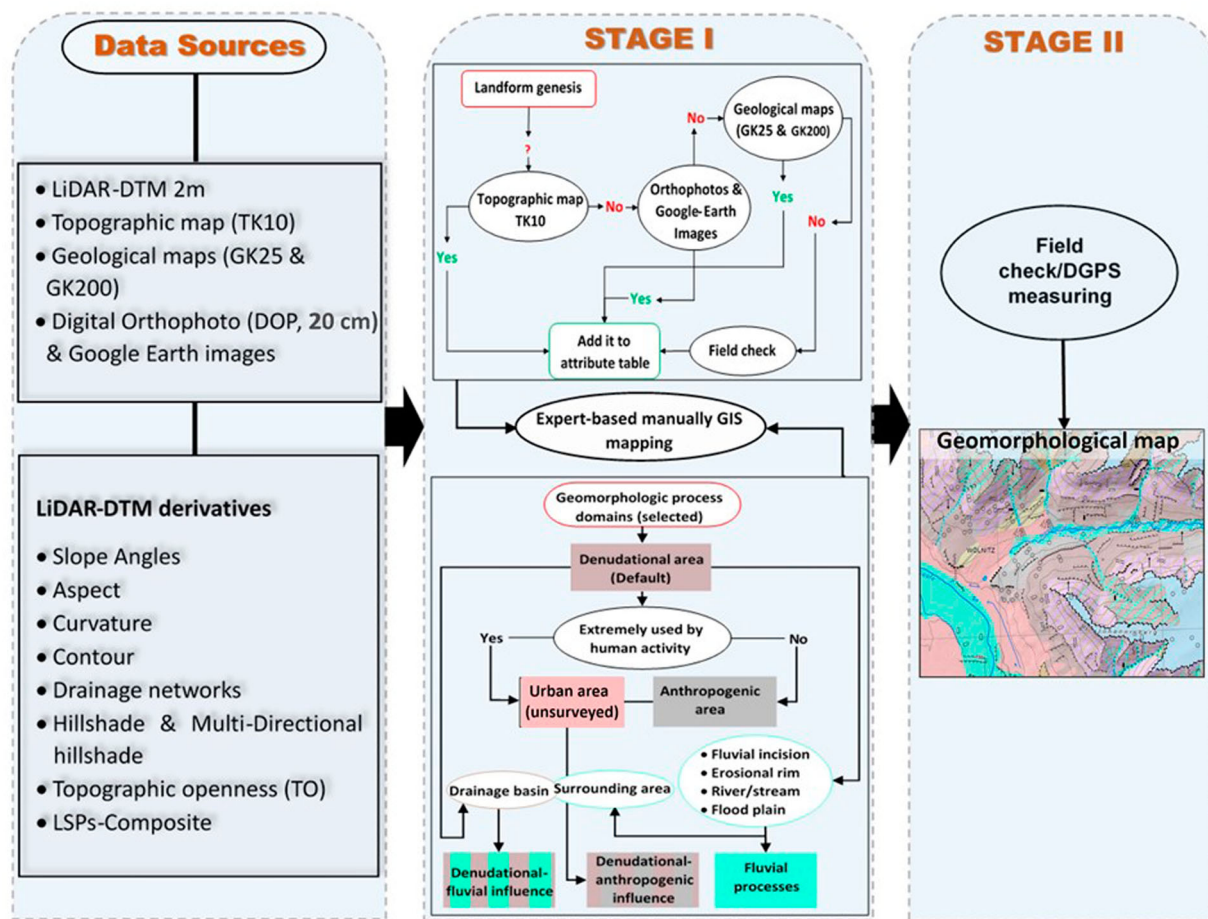


Figure 2. Flowchart showing the methodology used in this study.

existing scientific publications on the study area. The first field survey/pre-mapping was conducted at the beginning of the study to obtain a general overview of the landscapes, geomorphic processes, and landforms and to take some notes. The second survey was after the GIS-based/post-mapping to validate some features in the field with the aid of DGPS and to compare the efficacy of our method, using the combination of different data sources and the field-based mapping (refer to Figure 5). The Main Map was produced in ArcGIS 10.7 at a scale of 1:5000 with a Universal Transverse Mercator projection (Zone 32). The final map layout was chosen to fit an A0 format, requiring some degree of generalization (see Otto et al., 2011). For instance, many depressions and knoll-like landforms were substituted with point symbols instead of line symbols or were removed; however, any geomorphic domains that were too small to present on the final layout had to be replaced with the neighboring area or merged with the adjacent polygon. As an example, fluvial and denudational processes were merged into a single class by being denoted as of fluvial influence, in order to indicate the interaction between processes in a domain.

In addition, any delineated geomorphic processes (polygon features) at smaller scales were grouped or reproduced by their neighbor classes (Dramis et al.,

2011). This was manually executed; however, it is similar to the general concept of region-growing algorithms (Drăguț & Eisank, 2012). Furthermore, because of size and density of landforms, many steps and breaks in slope lines were subsequently removed or replaced with point symbols; for example, instead of presenting the steps of the incision by a line symbol, we employed a point symbol (Main Map, legend 3).

4. Results

Different geological formations have diverse and significant impacts on the landscapes of the Jena region. For instance, the northern part of the study area is dominated by limestone, which is characterized by escarpments, slopes, landslides, and v-shaped valleys. However, the southern part, dominated by sandstone, features several boxes and saucer-shaped valleys, flood plains, and terraces.

Some landforms were generalized or have been omitted for the final map to consider relevant landform visibility and improve readability. The final map is divided into four main classes/layers: geomorphological processes domains, hydrological features & pathways, hillslope processes & deposits, and topography & structural landforms.

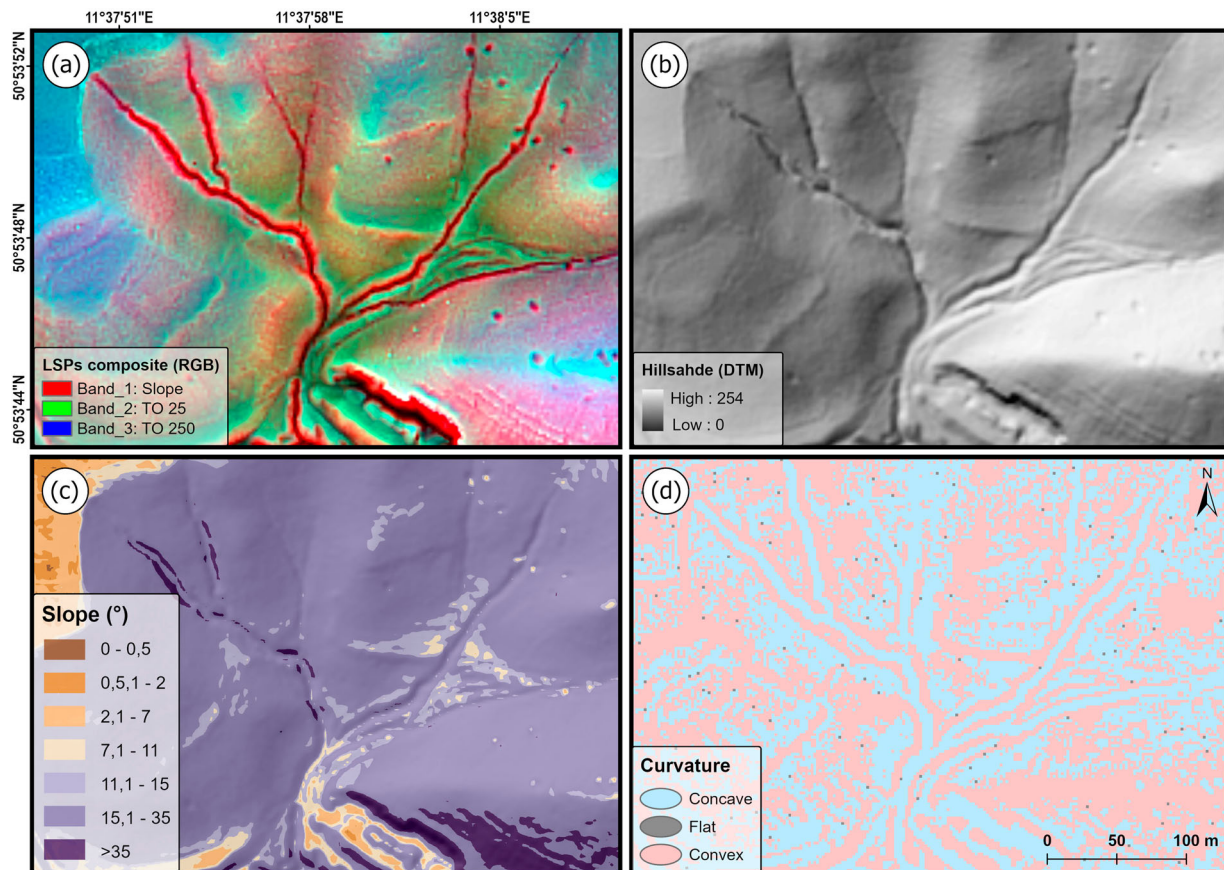


Figure 3. (a) LSPs composite map clearly defines landforms (bomb craters, queries, erosional rim...etc.) and their boundaries compared to DTM data and its derivatives, such as (b) hillshade, (c) slope, and (d) curvature.

4.1. Geomorphologic process domains

The northeastern part, the plateau, and the western part of the map edges, i.e. the high altitudes, are mostly dominated by karstic processes; however, rare karst features were also detected.

The northern and southern parts of the study area are dominated by the gravitational processes. The Kernberge, Johannisberg, Gräfenberg, and Einsiedlerberg mountain slopes are compatible with landslides, rock falls, creeps, and debris flows. The northeastern, central, and southern parts of the study area are dominated by denudational processes where other dynamic processes were not observed. The low-altitude zone and the valley slope areas are mostly characterized by fluvial processes, specifically along the Saale River and its tributaries. Fluvial–anthropogenic domains occur in the northwestern part, termed the Obere Aue area, and near Lobeda in the center of the map; i.e. the flood plain was modified by anthropogenic activities such as construction, and in the northeastern part of the area, the Pennickental river bed was influenced by mining activities.

Anthropogenic process domains are distributed all over the map. For instance, a part of Mönchsberg, the southwestern part of the area, was significantly altered by anthropogenic activity associated with the

Steinbruch quarry. As a result, a break in slope of approximately 30 m and a plateau of approximately 400 × 600 m was created.

The aeolian processes (loess accumulations) are not active in the area and ‘since loess in Europe was mainly accumulated during the cold stages of the Quaternary’ (Lehmkuhl et al., 2018), a clear distinction of the local extent of this class is not well defined in our area. It is presented on the map within sub-classes as it has been influenced by other processes. We identified loess accumulations on the eastern side of the Roda River, the western side of the Saale River, over the Spitzenberg Mountain slopes toward the Saale, and on the slopes toward the Ilmnitz, specifically between the contour lines of 175 and 225 m.

Periglacial processes are inactive in the study area and illustrated *via* the combination with other processes. It is mostly distributed along the hilly-mountain slope in the northern and southwestern parts of the map, where mainly dominated by the gravitation processes. The fluvial terraces occur along both flanks of the Saale and Roda channels, between 175 and 200 m asl. These terraces mostly undergo alteration by denudational and fluvial processes (see the Main Map, legend 1, for corresponding classes).

4.2. Hydrological features and pathways

The investigation area is mostly characterized by the Saale River valley and its tributaries. Perennial streams (e.g. Roda, Leutra, and Pennickental) and intermittent streams also contribute to terrain modification. In the northern part of the map, the Pennickental stream bed mostly undergoes alteration by anthropogenic activities (Section 4.1). Thus, the water is hampered to flow persistently and partially covers both stream flanks (Main Map, legend 2).

Various lakes with a range of sizes are distributed along the river and stream channels. For example, despite the trace of the Saale meander and the ridges of the old lakes, several lakes occur on the Saale active fluvial plain, near the southwestern corner of the map. The southern part of the study area is mostly covered by the sandstone formations dominated by saucer- and box-shaped valleys, whereas the northern part is controlled by limestone formations, where v-shaped valleys have mainly been investigated (see the Main Map, legend 2).

4.3. Hillslope processes and deposits

The central and northern parts of the study area are dominated by hills (e.g. Kernberge, Johannisberg, Gräfenberg, and Einsiedlerberg). The hill crests, which follow a west–east trend, are characterized by numerous incisions, and geomorphological evidence of rill erosion, rock falls and debris flows, especially in the slopes toward the Pennickental (e.g. Diebeskrippe landslide), the slopes toward the Saale, and the Einsiedlerberg slopes toward the south (see Section 4.1). In addition, on the southwestern part of the map, the mountain slopes of Mönchsberg, Jagdberg, and Spitzenberg to the Saale are dominated by a range of incisions, rill erosions, and rockfalls (Main Map, legend 3). Generally, the incision and rill erosion occur throughout the mapped area at a range of scales. Small alluvial fans occur at the mouth of the tributaries of Pennickental, in the northern part of the investigation area, and are mostly altered by shallow mass movements and anthropogenic activities.

4.4. Topography and structural landforms

The depressions are mainly distributed across the tops of the plateau landscape, located in the northern portion of the map; however, more specifically, they occur on the slopes of the Kernberge and Johanniseberg toward Wöllnitz, at the top of Mönchsberg (also Steinbruch), and its slopes toward the Winzerla, and on the slopes around Gräfenberg and Georgstein. Knoll/knob features (legend 4) mostly dominated the low-altitude (i.e. flat) areas along the Saale valley. Most exhibit a range of anthropogenic origins (see the Main Map,

legend 1) and are mostly modified by fluvial and denudational processes. Furthermore, steps and breaks in slope features occur throughout the mapped area; however, the northern portions of the map are extensively covered with mountainous areas, where the terrain is more complex than the southern part of the area.

Finally, most of the landforms and geomorphic process boundaries of the study area (e.g. plateau, mountains, valleys, catchments, terraces, and landslides) are controlled by crests, ridges, and breaks of slopes.

5. Discussion

This investigation supports evidence from previous observations (e.g. Jones et al., 2007; Roering et al., 2013) that reveal the accuracy of LiDAR data, showing that it is valuable for accelerated geomorphological mapping (Figure 5). Owing to the complex interactions between geomorphological processes in nature, a clear distinction between landforms solely from the remote sensing data was impossible. Therefore, Figure 1/Stage I illustrates our proposed approach as a step toward detecting landform geneses and geomorphological process domains by combining all data sources from on-screen mapping. Nonetheless, further developments could increase the extent of applicability of such pursuits, for instance, (1) by applying it to different environments and (2) by developing a novel approach to delineate and classify landform genesis automatically using DEMs based on LSPs (Seijmonsbergen et al., 2011).

We observed some discrepancies when overlaying different data sources, such as the topographic map and DOP with the DTMs. This occurs because of variations in scale as well as the date of data collection. For instance, anthropogenic activities such as roads, buildings, or construction may be represented only in some of the data, owing to different times of acquisition. Hence, utilizing data sources with the same scale and similar acquisition time is recommended (Otto & Smith, 2013). However, if the existing data sources do not fit to each other, which is hard to achieve, relying on the most recent data or conducting ground-truthing to illustrate current processes is more reliable.

The geological map enhanced on-screen mapping by providing adequate information to detect landform genesis, such as landslides with gravitational processes and terraces with fluvial processes (Figure 4). Nevertheless, a detailed boundary distinctions of landforms cannot be extracted from geological maps in contrast to their recognition from LSP composites and hillshade maps. This disagreement may reflect the lower scale of the geological map in comparison to the produced map. This research corroborates the ideas of Anders et al. (2011, 2015), Doneus (2013), Meng et al. (2018),

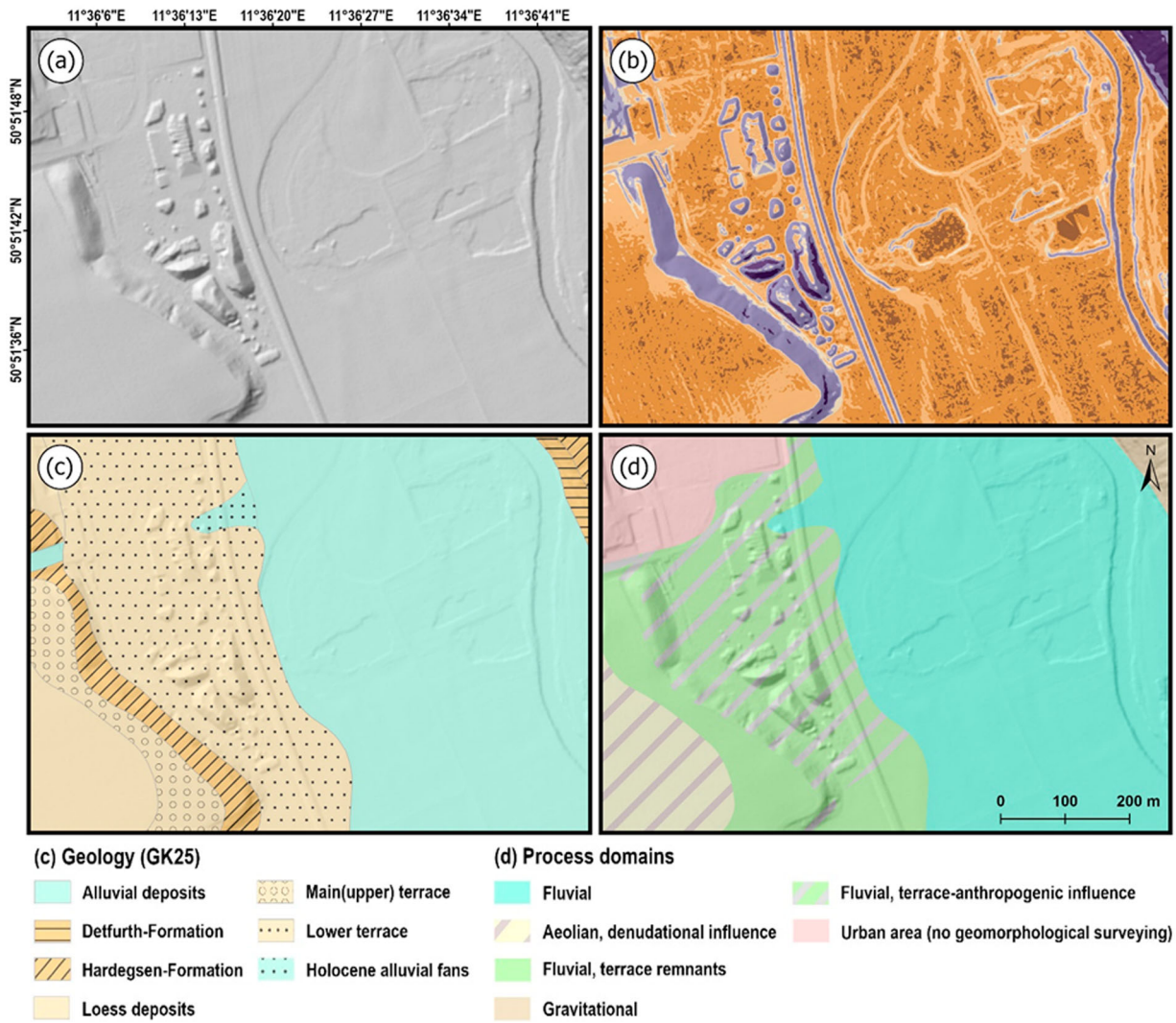


Figure 4. Example of process domain delineation (fluvial process): (a) Hillshade (for legend, see Fig. 3(b)). (b) slope, (for legend, see Fig. 3(c)). (c) geological map-GK25 and (d) the geomorphologic process domains.

and Daxer (2020), who suggested that TO and LSP composite maps are valuable for geomorphological mapping. This effort can be counted as an experiment toward an extension of the efficiency of that concept for manual mapping. In contrast, the slope map, which was classified based on the GMK25 legend (Main Map), is less suitable for a comprehensive representation of landforms. For example, Figure 3(c) indicates that most of the steps, incisions, bomb craters, and ridges are not fully represented based on this legend since the GMK25 legend was designed for a 1:25,000 scale map; however, not for a detailed scale such as 1:5000. Different classification intervals of slope angles were experienced in the initial steps when considering the general ideas of Jones et al. (2007), but further investigation is still needed, taking the map scale into account. In contrast to the traditional hillshade map, multidirectional hillshades promote the balance between over-exposed and non-illuminated areas of the map, resulting in a more realistic representation of the terrain (Nagi, 2014), and can further develop the accuracy of on-desktop mapping.

We validated the DTM-based GIS map with DGPS measurements in the field. Figure 5 indicates a good agreement between screen-based landforms and field checks related to the high resolution of digital base data for mapping. We observed an accuracy between a few millimeters (in most cases) to a meter or more (in seldom cases). However, mismatches between both approaches were observed. For example, in areas mostly covered by forest or vegetation, DGPS measuring was impossible. Some landforms were detected in the field but unidentifiable in LiDAR data. For example, hollows, knolls, and active processes such as sheet erosion or debris flows were not identified solely from the remotely sensed data. This can be due to the resolution of the DTM and the offset between acquisition times of digital and field data. Therefore, the resolution of digital data should be considered when a geomorphological map with higher precision and detailed scale is required. Therefore, the results presented here show that LiDAR data can quickly create a detailed geomorphological map of the middle-mountain environment but should not be

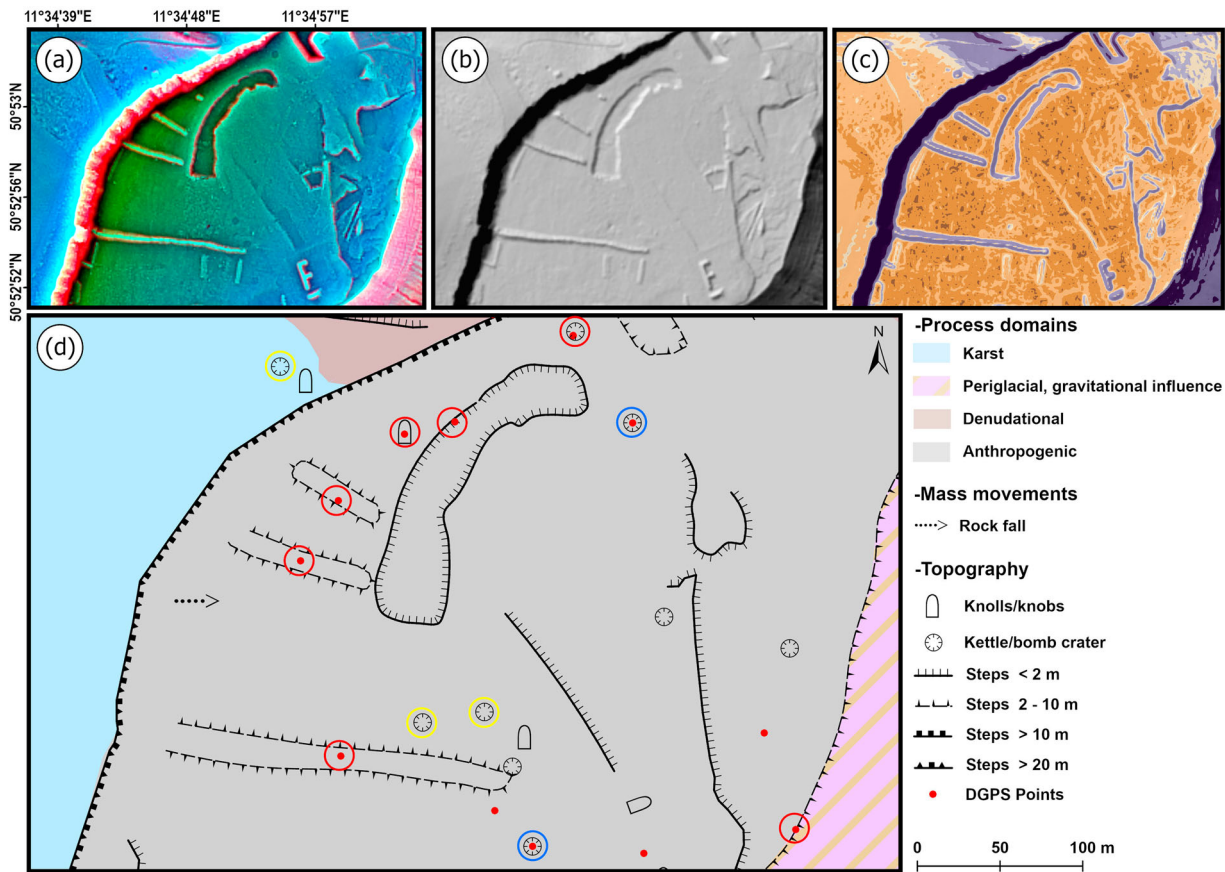


Figure 5. (a) LSPs-composite map, (b) hillshade, (c) the slope map of the Steinbruch quarry area, (d) an overview of the field/DGPS survey (red points). Red circles show that these landforms fit the DGPS measurements, and yellow circles present features that were not found in the field due to dense vegetation. Blue circles present landforms that could not be mapped by LiDAR-DTM-based on-screen analyses (see Fig. 3 for the legends of (a), (b), and (c) and Fig.1 for the location of this area).

considered a complete replacement for traditional methods.

6. Conclusion

This paper introduced a manual geomorphological map at a scale of 1:5000, based on ArcGIS tools and combining DTM, DTM derivatives, and LSPs-composite maps. Other inputs such as topographic maps, Google Earth images, DOPs, geological maps, and field examination were used to improve the mapping. This map can be used as a substitute approach geomorphological information from classical field-based maps.

Our approach provides high-accuracy layers of information. Moreover, the results obtained show that incorporating relevant LSPs, such as slope, curvature, elevation, multidirectional hillshade maps, and other derivatives such as TO and LSPs composite maps, provide valuable means of improving manually constructed digital geomorphological maps. Our proposed approach presents most geomorphological map layers and their properties at high quality; however, combining new layers of information or additional and better datasets might optimize the map.

We conclude that a combination of different data types, together with TO and LSPs, significantly enhances digital geomorphological mapping. Nevertheless, a field check of remotely sensed information still provides the best guarantee of producing accurate and updated high-resolution maps.

Google Earth images and DOP datasets with a resolution of approximately <20 cm are highly recommended for comprehensive mapping in flat and non-vegetated areas. The geological map can provide further improvement and flexible fine-tuning considering the genesis of some landforms (e.g. landslides and terraces). It is also valuable to determine the boundary of some geomorphological process domains (e.g. gravitational and fluvial processes). Notwithstanding, since the scale of the geological map is relatively smaller than that of the target map, uncertainties concerning the genesis of some landforms and their boundaries arose. Hence, geomorphological mapping can be enhanced when complemented with an equivalent resolution of geological data.

This approach is valuable for creating high-quality base data prior to or instead of field mapping, or when field survey time is limited. Furthermore, it provides a step forward in substituting traditional geomorphological

mapping approaches with on-screen digitized mapping, thereby presenting data sources for future studies in this area, despite its utility as a training sample for semi-automatic landform classification of typical landforms.

Our proposed approach can be applied in different environments to enhance the usability of geomorphological landforms and process domains.

Software

The dataset of the geomorphological map, including the morphometric analysis and the symbols of the map legend, has been digitized and managed, and the final design was obtained using ESRI ArcGIS 10.7, QGIS 3.16.3, ArcGIS Pro 2.6.2.

Open Scholarship



This article has earned the Center for Open Science badge for Open Data. The data are openly accessible at <https://doi.org/10.22000/798>.

Acknowledgements

This research is part of a Ph.D. project that aims to map middle-mountain geomorphology based on remote sensing data in Germany. We would like to acknowledge the financial support of the Human Capacity Development Program (HCDP) scholarship of the Ministry of Higher Education and Scientific Research-Kurdistan Regional Government (KRG) for this project. The authors would like to thank Simon Terweh for his support during the DGPS analysis. We also thank Paolo Magliulo, Elizabeth Rudolph and Jessica Baker for valuable comments that helped to improve the manuscript and map.

Disclosure statement

No potential conflict of interest was reported by the author(s).

Funding

This work was supported by the Open Access Publication Fund of the University of Bonn.

ORCID

Ikram Zangana  <http://orcid.org/0000-0003-4998-8577>
Jan-Christoph Otto  <http://orcid.org/0000-0002-4552-3011>

References

Anders, N. S., Seijmonsbergen, A. C., & Bouten, W. (2011). Segmentation optimization and stratified object-based analysis for semi-automated geomorphological mapping. *Remote Sensing of Environment*, 115(12), 2976–2985. <https://doi.org/10.1016/j.rse.2011.05.007>

- Anders, N. S., Seijmonsbergen, A. C., & Bouten, W. (2015). Rule set transferability for object-based feature extraction: An example for cirque mapping. *Photogrammetric Engineering & Remote Sensing*, 81(6), 507–514. <https://doi.org/10.14358/PERS.81.6.507>
- Barsch, D., & Liedtke, H. (1985). *Geomorphological mapping in the Federal Republic of Germany* (H 39, pp. 1–94). Berliner Geographische Abhandlungen.
- Beckenbach, E., Müller, T., Seyfried, H., & Simon, T. (2014). Potential of a high-resolution DTM with large spatial coverage for visualization, identification and interpretation of young (Würmian) glacial geomorphology. *Quaternary Science Journal*, 63(2), 107–129. <https://doi.org/10.3285/eg.63.2.01>
- Blaschke, T. (2010). Object based image analysis for remote sensing. *ISPRS Journal of Photogrammetry and Remote Sensing*, 65(1), 2–16. <https://doi.org/10.1016/j.isprsjprs.2009.06.004>
- Bollati, I., Crosa Lenz, B., Zanoletti, E., & Pelfini, M. (2017). Geomorphological mapping for the valorization of the alpine environment. A methodological proposal tested in the Loana Valley (Sesia Val Grande Geopark, Western Italian Alps). *Journal of Mountain Science*, 14(6), 1023–1038. <https://doi.org/10.1007/s11629-017-4427-7>
- Chandler, B. M. P., Lovell, H., Boston, C. M., Lukas, S., Barr, I. D., Benediktsson, ÍÖ, Benn, D. I., Clark, C. D., Darvill, C. M., Evans, D. J.A., Ewertowski, M. W., Loibl, D., Margold, M., Otto, J.-C., Roberts, D. H., Stokes, C. R., Storrar, R. D., & Stroeven, A. P. (2018). Glacial geomorphological mapping: A review of approaches and frameworks for best practice. *Earth-Science Reviews*, 185 (November 2017), 806–846. <https://doi.org/10.1016/j.earscirev.2018.07.015>
- Chen, H., Oguchi, T., & Wu, P. (2018). Morphometric analysis of sinkholes using a semi-automatic approach in Zhijin County, China. *Arabian Journal of Geosciences*, 11(2), 15. <https://doi.org/10.1007/s12517-017-3379-0>
- Daxer, C. (2020). *Topographic openness maps and Red relief image maps in QGIS* (Tech. Rep.). Institute of Geology. <https://doi.org/10.13140/RG.2.2.18958.31047>
- Devoto, S., Biolchi, S., Bruschi, V. M., Furlani, S., Mantovani, M., Piacentini, D., Pasuto, A., & Soldati, M (2012). Geomorphological map of the NW Coast of the Island of Malta (Mediterranean Sea). *Journal of Maps*, 8(1), 33–40. <https://doi.org/10.1080/17445647.2012.668425>
- Doneus, M. (2013). Openness as visualization technique for interpretative mapping of airborne lidar derived digital terrain models. *Remote Sensing*, 5(12), 6427–6442. <https://doi.org/10.3390/rs5126427>
- Dräguţ, L., & Eisank, C. (2012). Automated object-based classification of topography from SRTM data. *Geomorphology*, 141–142, 21–33. <https://doi.org/10.1016/j.geomorph.2011.12.001>
- Dramis, F., Guida, D., & Cestari, A. (2011). Nature and aims of geomorphological mapping. In M. J. Smith, P. Paron, & J. Griffiths (Eds.), *Geomorphological Mapping: methods and applications* (Vol. 15, pp. 39–73). Elsevier. <https://doi.org/10.1016/B978-0-444-53446-0.00003-3>
- Föhlisch, K. (2002). *Synsedimentäre Deformationen im Unteren Muschelkalk des Germanischen Beckens* [Dissertation zur Erlangung des akademischen Grades doctor rerum naturalium]. Friedrich-Schiller-Universität Jena. Online: <https://nbn-resolving.org/urn:nbn:de:gbv:27-dbt-000767-3>

- Garcia, G. P. B., & Grohmann, C. H. (2019). DEM-based geomorphological mapping and landforms characterization of a tropical karst environment in southeastern Brazil. *Journal of South American Earth Sciences*, 93 (March), 14–22. <https://doi.org/10.1016/j.jsames.2019.04.013>
- Gehrmann, A., & Harding, C. (2018). Geomorphological mapping and spatial analyses of an upper Weichselian Glacitectonic complex based on LiDAR data, Jasmund Peninsula. *Geosciences*, 8(208), 1–24. <https://doi.org/10.3390/geosciences8060208>
- Gustavsson, M., Kolstrup, E., & Seijmonsbergen, A. C. (2006). A new symbol-and-GIS based detailed geomorphological mapping system: Renewal of a scientific discipline for understanding landscape development. *Geomorphology*, 77(1–2), 90–111. <https://doi.org/10.1016/j.geomorph.2006.01.026>
- Gustavsson, M., Seijmonsbergen, A. C., & Kolstrup, E. (2008). Structure and contents of a new geomorphological GIS database linked to a geomorphological map – With an example from Liden, central Sweden. *Geomorphology*, 95(3–4), 335–349. <https://doi.org/10.1016/j.geomorph.2007.06.014>
- Hengl, T., & Reuter, H. I. (2008). *Geomorphometry: Concepts, software, applications. Developments in soil science*. Elsevier. [https://doi.org/10.1016/S0166-2481\(07\)32042-4](https://doi.org/10.1016/S0166-2481(07)32042-4)
- Hillier, J. K., Smith, M. J., Armugam, R., Barr, I., Boston, C. M., Clark, C. D., Ely, J., Frankl, A., Greenwood, S.L., Gosselin, L., Hättestrand, C., Hogan, K., Hughes, A.L.C., Livingstone, S.J., Lovell, H., McHenry, M., Munoz, Y., Pellicer, X.M., Pellitero, R., ... Wooldridge, K. (2015). Manual mapping of drumlins in synthetic landscapes to assess operator effectiveness. *Journal of Maps*, 11(5), 719–729. <https://doi.org/10.1080/17445647.2014.957251>
- Jones, A. F., Brewer, P. A., Johnstone, E., & Macklin, M. G. (2007). High-resolution interpretative geomorphological mapping of river valley environments using airborne LiDAR data. *Earth Surface Processes and Landforms*, 32 (10), 1574–1592. <https://doi.org/10.1002/esp.1505>
- Lambiel, C., Maillard, B., Kummert, M., & Reynard, E. (2016). Geomorphology of the Hérens valley (Swiss Alps). *Journal of Maps*, 12(1), 160–172. <https://doi.org/10.1080/17445647.2014.999135>
- Lehmkuhl, F., Pötter, S., Pauligk, A., & Böskén, J. (2018). Loess and other quaternary sediments in Germany. *Journal of Maps*, 14(2), 330–340. <https://doi.org/10.1080/17445647.2018.1473817>
- MacMillan, R. A., & Shary, P. A. (2009). Landforms and landform elements in geomorphometry. In T. Hengl & R. I. Hannes (Eds.), *Developments in soil science* (Vol. 33, pp. 227–254). Elsevier. [https://doi.org/10.1016/S0166-2481\(08\)00009-3](https://doi.org/10.1016/S0166-2481(08)00009-3)
- Magliulo, P., & Valente, A. (2020). GIS-based geomorphological map of the Calore River floodplain near Benevento (Southern Italy) overflowed by the 15th October 2015 event. *Water*, 12(1), 148. <https://doi.org/10.3390/w12010148>
- Mcdowell, P. F. (2013). Geomorphology in the late twentieth century. In J. E. Shroder, A. R. Orme, & D. Sack (Eds.), *Treatise on geomorphology* (Vol. 1, pp. 108–123). <https://doi.org/10.1016/B978-0-12-374739-6.00007-5>
- Meng, X., Xiong, L. Y., Yang, X. W., Yang, B. S., & Tang, G. A. (2018). A terrain openness index for the extraction of Karst Fenglin and Fengcong landform units from DEMs. *Journal of Mountain Science*, 15(4), 752–764. <https://doi.org/10.1007/s11629-017-4742-z>
- Nagi, R. (2014). *Multi-directional Hillshade makes your maps pop*. Retrieved March 12, 2020, from <https://www.esri.com/about/newsroom/wp-content/uploads/2018/10/multi-directional-hillshade-makes-your-maps-pop.pdf>
- Napiersalski, J., Barr, I., Kamp, U., & Kervyn, M. (2013). Remote sensing and GIScience in geomorphological mapping. In J. F. Shroder & M. P. Bishop (Eds.), *Treatise on geomorphology* (Vol. 3, pp. 187–227). Elsevier. <https://doi.org/10.1016/B978-0-12-374739-6.00050-6>
- Otto, J.-C. (2008). *Symbols for geomorphologic mapping in high mountains for ArcGIS*. http://www.geomorphology.at/index.php?option=com_content&task=view&id=133&Itemid=176
- Otto, J.-C., & Dikau, R. (2004). Geomorphologic system analysis of a high mountain valley in the Swiss Alps. *Zeitschrift Für Geomorphologie*, 48, 323–341. Berlin, Stuttgart.
- Otto, J. C., Gustavsson, M., & Geilhausen, M. (2011). Cartography. Design, symbolisation and visualisation of geomorphological maps. In Smith M. J., Paron P., & Griffiths J. S. (Eds.), *Geomorphological mapping: Methods and applications* (Vol. 15, pp. 253–295). Elsevier. <https://doi.org/10.1016/B978-0-444-53446-0.00009-4>
- Otto, J.-C., Prasicek, G., Blöthe, J., & Schrott, L. (2017). GIS applications in geomorphology. In B. Haug (Ed.), *Comprehensive geographic information systems* (Vol. A2, pp. 81–111). Elsevier. <https://doi.org/10.1016/B978-0-12-409548-9.10029-6>
- Otto, J.-C., & Smith, M. J. (2013). Section 2.6: Geomorphological mapping. In L. E. Clarke & J. M. Neild (Eds.), *Geomorphological techniques (online edition)* (Vol. 6, pp. 1–10). British Society for Geomorphology.
- Parry, S. (2011). The application of geomorphological mapping in the assessment of landslide hazard in Hong Kong. In M. J. Smith, P. Paron, & J. S. Griffiths (Eds.), *Geomorphological mapping: Methods and applications* (Vol. 15, pp. 413–441). Elsevier. <https://doi.org/10.1016/B978-0-444-53446-0.00015-X>
- Piloyan, A., & Konečný, M. (2017). Semi-automated classification of landform elements in Armenia based on SRTM DEM using K-means unsupervised classification. *Quaestiones Geographicae*, 36(1), 93–103. <https://doi.org/10.1515/quageo-2017-0007>
- Rau, D., Schramm, H., & Wunderlich, J. (2000). *Legende zur Bodengeologischen Konzeptkarte Thüringens i. M. 1 : 100 000*. Thüringer Landesanstalt für Geologie.
- Roering, J. J., Mackey, B. H., Marshall, J. A., Sweeney, K. E., Deligne, N. I., Booth, A. M., Handwerker, A. L., & Cerovski-Darriau, C. (2013). “You are HERE”: Connecting the dots with airborne lidar for geomorphic fieldwork. *Geomorphology*, 200, 172–183. <https://doi.org/10.1016/j.geomorph.2013.04.009>
- Schneevoigt, N. J., van der Linden, S., Thamm, H. P., & Schrott, L. (2008). Detecting Alpine landforms from remotely sensed imagery. A pilot study in the Bavarian Alps. *Geomorphology*, 93(1–2), 104–119. <https://doi.org/10.1016/j.geomorph.2006.12.034>
- Schrott, L., Otto, J.-C., Götz, J., & Geilhausen, M. (2013). Fundamental classic and modern field techniques in geomorphology: An overview. *Treatise on Geomorphology*, 14, 6–21. <https://doi.org/10.1016/B978-0-12-374739-6.00369-9>
- Seidel, G. (1992). *Sammlung geologischer Führer-Thüringer Becken* (85th ed). Bornträger.
- Seijmonsbergen, A. C. (2013). The modern geomorphological map. In J. F. Shroder, A. D. Switzer, & D. M. Kennedy

- (Eds.), *Treatise on geomorphology* (Vol. 14, pp. 35–52). Elsevier. <https://doi.org/10.1016/B978-0-12-374739-6.00371-7>
- Seijmonsbergen, A. C., Hengl, T., & Anders, N. S. (2011). Semi-automated identification and extraction of geomorphological features using digital elevation data. In M. J. Smith, P. Paron, & J. S. Griffiths (Eds.), *Geomorphological mapping: Methods and applications* (Vol. 15). Elsevier. <https://doi.org/10.1016/B978-0-444-53446-0.00010-0>
- Skentos, A. (2018). Combining digital elevation data, expert knowledge and GIS for geomorphological mapping: The case study of Mount Hymettus, Athens, Greece. *Annals of Valahia University of Targoviste, Geographical Series*, 18 (1), 23–32. <https://doi.org/10.2478/avutgs-2018-0003>
- Smith, M. J. (2011). Digital mapping: Visualisation, interpretation and quantification of landforms. In M. J. Smith, P. Paron, & J. S. Griffiths (Eds.), *Geomorphological mapping: Methods and applications* (Vol. 15, pp. 225–251). Elsevier. <https://doi.org/10.1016/B978-0-444-53446-0.00008-2>
- Smith, M. J., & Clark, C. D. (2005). Methods for the visualization of digital elevation models for landform mapping. *Earth Surface Processes and Landforms*, 30(7), 885–900. <https://doi.org/10.1002/esp.1210>
- Smith, M. J., Hillier, J. K., Otto, J.-C., & Geilhausen, M. (2013). Geovisualization. In J. Shroder & M. P. Bishop (Eds.), *Treatise on geomorphology* (pp. 299–325). <https://doi.org/10.1016/B978-0-12-374739-6.00054-3299>
- Smith, M. J., & Pain, C. F. (2009). Applications of remote sensing in geomorphology. *Progress in Physical Geography: Earth and Environment*, 33(4), 568–582. <https://doi.org/10.1177/0309133309346648>
- Smith, M. J., Paron, P., & Griffiths, J. S. (2011). *Geomorphological mapping: Methods and applications*. Elsevier.
- TLBG. (2019a). *Digitale Geländemodelle (DGM)*. <https://www.geoportal-th.de/de-de/Downloadbereiche/Download-Offene-Geodaten-Thüringen/Download-Höhendaten>
- TLBG. (2019b). *Digitale Orthophotos (DOP)*. <https://www.geoportal-th.de/de-de/Downloadbereiche/Download-Offene-Geodaten-Thüringen/Download-Luftbilder-und-Orthophotos>
- TLBG. (2019c). *Digitale Topographische Karte 1:10.000 (DTK10)*. <https://www.geoportal-th.de/de-de/Downloadbereiche/Download-Offene-Geodaten-Thüringen/Download-Topographische-Karten>
- TLUBN. (2019). *Digitale Geologische Karte von Thüringen für den Maßstab 1: 25.000 (GK25digTh)*. <http://antares.thueringen.de/cadenza/pages/map/default/index.xhtml;jsessionid=5DF262BE272F1E39739A87B3A8F4F458>
- TLUBN. (2022). *Landnutzung*. https://antares.thueringen.de/cadenza/pages/map/default/index.xhtml;jsessionid=C40D8C95596E44DA65325F3E8DA7F2AC?mapId=da191d35-5f45-4c97-8247-202c2371293f&repositoryItemGlobalId=Anwendungen.basiskarte_topo.mml&mapSrs=EPSG%3A25832&mapExtent=680094.62471
- TMUEN. (2017). *Klimawandelfolgen in Thüringen Monitoringbericht 2017*. <https://www.thueringen.de/de/publikationen/pic/pubdownload1708.pdf>
- Tzvetkov, J. (2018). Relief visualization techniques using free and open source GIS tools. *Polish Cartographical Review*, 50(2), 61–71. <https://doi.org/10.2478/pcr-2018-0004>
- Wood, J. D. (1996). *The geomorphological characterisation of digital elevation models* [Doctoral dissertation]. University of Leicester. [https://doi.org/10.1016/S0065-230X\(09\)04001-9](https://doi.org/10.1016/S0065-230X(09)04001-9)
- Wu, Q., Deng, C., & Chen, Z. (2016). Automated delineation of karst sinkholes from LiDAR-derived digital elevation models. *Geomorphology*, 266, 1–10. <https://doi.org/10.1016/j.geomorph.2016.05.006>